

We are IntechOpen, the world's leading publisher of Open Access books Built by scientists, for scientists

6,900

Open access books available

186,000

International authors and editors

200M

Downloads

Our authors are among the

154

Countries delivered to

TOP 1%

most cited scientists

12.2%

Contributors from top 500 universities



WEB OF SCIENCE™

Selection of our books indexed in the Book Citation Index
in Web of Science™ Core Collection (BKCI)

Interested in publishing with us?
Contact book.department@intechopen.com

Numbers displayed above are based on latest data collected.
For more information visit www.intechopen.com



Structural and Electronic Properties of Hydrogenated Graphene

Duminda K. Samarakoon and Xiao-Qian Wang

Department of Physics and Center for Functional Nanoscale Materials, Clark Atlanta University, Atlanta, Georgia 30314 USA

1. Introduction

1.1 Overview

Graphane is a two-dimensional system consisting of a single planar layer of fully saturated carbon atoms, which has recently been realized experimentally through hydrogenation of graphene membranes. In this chapter, we categorize theoretical approaches using the first-principles calculations, and we discuss in some detail our applications of calculation approaches to graphane systems. Specifically, we have studied the stability of chair, boat, and twist-boat graphane structures. Our results indicate that locally stable twist-boat membranes significantly contribute to the experimentally observed lattice contraction. The band gaps of graphane nanoribbons decrease monotonically with the increase of the ribbon width and are insensitive to the edge structure. We have also studied the electronic structural characteristics in a hydrogenated bilayer graphene under a perpendicular electric bias. The bias voltage applied between the two hydrogenated graphene layers allows continuously tuning the band gap and leads a transition from semiconducting to metallic state. Desorption of hydrogen from one layer in the chair conformation yields a ferromagnetic semiconductor with tunable band gap. Finally, we offer some views on the strength and weakness of the approaches that are discussed, and touch upon some of the challenging problems that need to be addressed in the future.

1.2 Graphene and graphane

Graphene, a single layer of all-carbon hexagonal network, is an emerging material for applications in electronics and photonics Berger et al. (2006); Geim & Novoselov (2007); Geim et al. (2007); Gilje et al. (2007); Novoselov et al. (2005); Wang et al. (2008); Zhang et al. (2006). As a truly two-dimensional system and a zero-gap semiconductor where the carriers behave as massless fermions, graphene possesses a number of outstanding electronic properties such as tunable carrier type and density Berger et al. (2006), exceptionally high carrier mobility Zhang et al. (2006), quantization of the conductivity Novoselov et al. (2005), and fractional quantum Hall effect (QHE) even at room temperature Zhang et al. (2005). These phenomena, particularly the QHE Zhang et al. (2005), have elucidated many important aspects of quantum many-body systems Zhang et al. (2005). The corresponding electronic states in graphene promote theoretical advances Ciftja & Fantoni (1996); Halperin et al. (1993); Jain (1989); Laughlin (1983) in studying strongly correlated Dirac fermions. Functionalizing

graphene by reversible hydrogenation can change the electronic properties from metallic to semiconducting owing to the induced changes of functionalized carbon from sp^2 to sp^3 hybridization Geim et al. (2007); Gilje et al. (2007); Wang et al. (2008). The resultant hydrocarbon compound, graphane, can be modified into new materials, fine tuning its electronic properties, and has opened up increasingly fertile possibilities in hydrogen storage and two dimensional electronics Berger et al. (2006); Geim & Novoselov (2007); Geim et al. (2007); Gilje et al. (2007); Novoselov et al. (2005); Wang et al. (2008); Zhang et al. (2006).

1.3 Energy gaps

To develop increasingly small and fast transistors, it is desirable to have an energy gap Berger et al. (2006); Zhang et al. (2006). In contrast to complicated graphene-based structures like quantum point contacts and quantum dots, chemical derivatives of graphene provide a unique tool for controlling electronic properties Gilje et al. (2007). In order to utilize their remarkable electronic characteristics, it would be highly desirable to understand the associated electronic structures. Based on first-principles density-functional calculations, the stability and semiconducting behavior of graphane, an extended two dimensional fully saturated hydrocarbon derived from a single graphene sheet Boukhvalov et al. (2008); Sofu et al. (2007), was predicted. Recent experiments Elias et al. (2009) demonstrated the graphane formation by exposing pristine graphene to atomic hydrogen. There exist drastic changes in the crystal structure of graphane such that the lattice spacing shrinks by as much as 5% whereas the hexagonal symmetry remains intact.

The experimentally observed lattice spacing Elias et al. (2009) has a significantly broader variation than theoretically studied conformations of graphane Boukhvalov et al. (2008); Sofu et al. (2007). Theoretical work has considered two conformations: a chair like conformer in which hydrogen atoms are alternating on both sides of the plane, and a boat like conformer in which hydrogen atoms are alternating in pairs Boukhvalov et al. (2008); Sofu et al. (2007). In the ground state chair conformation of graphane, hydrogen attaches to graphene sublattices from two opposite sides and carbon atoms in the sublattices move out of the plane that yields the shrinkage of the in-plane periodicity. However, the change in hybridization from sp^2 to sp^3 leads to longer C-C bonds, which surpasses the lattice shrinkage by chair membrane buckling. The experimental observation of more compressed areas implies the existence of alternative membranes in the crystal structures of graphane, which results in stronger membrane buckling and shorter in-plane lattice spacing Elias et al. (2009).

We have performed a comprehensive investigation of structural and electronic properties of the graphane and graphane nanoribbons. We employ a combination of classical molecular dynamics Tersoff (1988) and first-principles density-functional approach. Kresse & Furthmuller (1996) Classical molecular dynamics was used to pre-screen molecular geometries, and first-principles calculations were employed to determine the electronic structure. Our results indicate that the locally stable twist-boat membranes lead to pronounced lattice shrinkage, and thus contribute to the broader distribution of lattice spacing observed experimentally Elias et al. (2009). The incorporation of twist-boat membranes into the crystal structure of graphane is shown to preserve the semiconducting feature of graphane. Furthermore, a systematic study of the graphane nanoribbons shows the band gaps of graphane nanoribbons decrease monotonically with the increase of the ribbon width and are insensitive to the edge structure.

1.4 Bilayer graphane

Graphene is a one-layer sheet of carbon with a structure that resembles chicken wire. Graphene has proven to possess unique electronic and physical properties, such as the unconventional quantum Hall effect Zhang et al. (2006), and high carrier mobility at room temperature Berger et al. (2006); Neto et al. (2009); Novoselov et al. (2004), thereby holding potential for a wide range of applications including graphene transistors, integrated circuits, and biosensors Berger et al. (2006); Neto et al. (2009); Novoselov et al. (2004); Zhang et al. (2006). The quantum-Hall effect Tsui et al. (1982) and the associated strongly correlated electron systems have generated a tremendous impetus on the development of novel ideas in many-body physics like the existence of fractionally charged quasiparticles Laughlin (1983), topological quantum numbers Thouless (1998), chiral Luttinger liquids Wen (1990; 1991), composite fermion particles Ciftja (2000); Jain (1989), and Chern-Simmons effective-field theories Ciftja & Wexler (2001); Halperin et al. (1993). Bringing graphene up to the level of technologically relevant material, however, depends on improved understanding and control of the structural and electronic properties. Specifically, an energy gap can be engineered by introducing lateral confinement such as in graphene nanoribbons Li et al. (2008); Nduwimana & Wang (2009), hydrogenated graphene Elias et al. (2009); Guisinger et al. (2009); Sofo et al. (2007), or in biased bilayer graphene Castro et al. (2007; 2008); Mak et al. (2009); McCann (2006); Min et al. (2007); Nilsson et al. (2008); Ohta et al. (2006); Oostinga et al. (2008); Zhang et al. (2009). The engineering of band gaps generates a pathway for possible graphene-based nanoelectronic and nanophotonic devices.

The extremely high carrier mobility makes graphene an ideal material for nanoelectronic applications, especially in field effect transistors Berger et al. (2006); Neto et al. (2009); Novoselov et al. (2004). Although graphene nanoribbon field effect transistors have been shown to exhibit excellent properties Li et al. (2008), mass production of graphene nanoribbon-based devices is beyond the capability of current lithography technology Nilsson et al. (2008). An alternative route to induce the formation of a band gap is through the hydrogenation of graphene Elias et al. (2009); Guisinger et al. (2009). The modification of the carbon bonds associated with the hydrogenation preserves the crystalline order of the lattice, but leads to re-hybridization of the carbon atoms from a planar sp^2 to a distorted sp^3 state Sofo et al. (2007). Recent experimental studies have demonstrated reversible hydrogenation through heating and proceeding with de-hydrogenation of the graphane to graphene Elias et al. (2009). On the other hand, bilayer graphene has attracted a great deal of attention recently. In bilayer graphene, the low energy excitations are one of the characteristics of massive chiral fermions, unlike Dirac fermions in graphene Novoselov et al. (2005). Most importantly, bilayer graphene can have a tunable gap *via* chemical doping or by applying an external gate voltage. In lieu of the increasing amount of experimental and theoretical studies of the bilayer graphene transistors Xia et al. (2010), the exploration of various modified bilayer systems could play a crucial role in future nanoelectronics applications.

Experimental advances have motivated our study of what could emerge if bilayer graphene were subjected to hydrogenation and electric bias. We have investigated the corresponding bilayer systems based on first-principles density-functional calculations. Fully-hydrogenated bilayer graphene is similar to the one-layer graphene in that the electronic properties change from metallic to the semiconductive due to the induced changes of functionalized carbon from sp^2 to sp^3 hybridization, and the interlayer chemical bonding that stabilizes the hydrogenated structure Leenaerts et al. (2009). We show that with applied electric bias, the resultant energy gap can be tuned. Of particular interest are the effects associated with symmetry breaking due to the presence of an external electric field perpendicular to the hydrogenated bilayer

graphene. Our theoretical study suggests a unique opportunity to tune the band gap of a ferromagnetic semiconductor with desorption of hydrogen from one layer in the chair conformation.

The chapter is organized as follows. In Section 2 we discuss the first-principles calculation method employed. In Section 3, we describe in detail the study of lattice contraction observed experimentally, through careful examinations of chair, boat, and twist-boat membranes. We then investigate the effect of electric bias on the bilayer graphene. Finally, in Section 4 we summarize our theoretical simulation work.

2. Method

2.1 First-principles calculations

Although first-principle methods are generally more reliable than the empirical methods, they are currently limited to small systems (a few hundred atoms). Recently, several groups have developed methods for performing first-principles electronic structure calculations that scale linearly with system size (the $O(N)$ methods). These methods are now applicable to systems that could only be studied by means of empirical and semi-empirical methods a decade ago. Moreover, the relative reduction in computational cost enables the molecular-dynamics simulations and therefore the investigation of complicated physical and chemical systems.

Recent advances in *ab initio* methods have experienced a considerable amount of success in predicting ground-state structural and cohesive properties of condensed-matter systems. The pioneering work of Car and Parrinello based on dynamical simulated annealing promoted a new type of approach applicable to density-functional theory within the local-density approximation (LDA). Density-functional molecular dynamics (Car-Parrinello) and other iterative methods based on plane-wave basis have made such calculations possible for systems consisting of several hundred atoms.

Most of contemporary LDA calculations are based on the Kohn-Sham formulation. LDA provides structural and elastic data in good agreement with experiment; lattice constants, bulk modules, elastic constants and phonon frequencies are usually predicted within 5% of experimental values. For binding energies, LDA consistently overestimates experimental values by approximately 10-20%. This error is attributed to the incomplete cancelation of errors within the LDA method. While these methods have been very successful, several difficulties arise when they are extended to systems with large length scales or those containing transition-metal atoms.

The first-principles methods based on plane-wave basis sets require many components in the expansion to keep track of the locality of the electronic wave functions. In the plane-wave basis, the kinetic energy operator is diagonal while the potential energy matrix is not sparse. In contrast, both the kinetic energy and potential energy matrix are approximately band-diagonal in the wavelet basis. Moreover, the wavelet transform, along with the associated multiresolution analysis, does not involve long-range operations and is thus particularly suitable for parallelization and wave-function-based $O(N)$ algorithms, since every operation can be partitioned into hierarchical real-space domains. In the following, we briefly discuss the density functional theory, the first-principles molecular dynamics, code developments, and the wavelet bases for electronic structure calculations.

2.2 Density functional theory

To properly handle a many-electron system so that one can derive its various properties from fundamental quantum mechanics is a constant challenge in theoretical physics and chemistry.

Although the interaction between electrons is well known, the facts that electrons, with a spin quantum number of 1/2, have to obey specific statistical rules and that one normally has to deal with quite a few of them at the same time make this problem immensely formidable. One approach that has become the standard one for large-scale electronic simulations is the density functional theory in the so-called Kohn-Sham framework. It is based on a theorem stating that the ground-state energy of a many-electron system can be represented as a functional of the electron density only. As a result, one can obtain the electronic energy without dealing with the many-body wave function which is highly multidimensional with the notorious property of being antisymmetric with respect to particle exchange. Being a scalar in the real space, the electron density is a much simpler quantity to manage, making it possible to investigate more complex systems. By minimizing the energy functional with respect to possible density distributions one can then determine the ground-state electronic energy for a given atomic arrangement.

The energy minimization procedure is most conveniently carried out by a mapping of the truly interacting system to an auxiliary system of noninteracting particles with the same density distribution. The resulting total-energy functional

$$E[n] = T_0[n] + \int d^3r v_{ext}(\mathbf{r}) n(\mathbf{r}) + E_h[n] + E_{xc}[n] \quad (1)$$

includes the kinetic energy functional of the noninteracting system $T_0[n]$, external potential energy, Hartree energy $E_h[n]$, and the so-called exchange-correlation energy functional $E_{xc}[n]$. $E_{xc}[n]$ includes all the many-body effect as well as the difference in the kinetic energies of the interacting and noninteracting systems.

The direct variation of energy with respect to the density is replaced by finding the noninteracting orbitals ψ self-consistently in the local Kohn-Sham equations

$$\left(-\frac{\hbar^2}{2m}\nabla^2 + V_{ext} + V_{eff}\right)\psi_i = \varepsilon_i\psi_i, \quad (2)$$

where the effective one-particle potential V_{eff} includes the Hartree potential and the exchange-correlation potential derived from a functional derivative $V_{xc} = \delta E_{xc}/\delta n$. The density is calculated from all occupied one-particle orbitals. The fact that the effective potential is a simple local function makes a tremendous difference in practical calculations. Other quantum-chemistry schemes such as the Hartree-Fock method commonly involves nonlocal operators which require much more computational resources. It is ok that the density-functional theory has become the prevailing approach in modern electronic-structure calculations with wide applications in quantum chemistry and materials physics.

Inarguably one could not have solved the exact many-body problem by regrouping energy terms. As a matter of fact, although the existence of the exchange-correlation energy functional E_{xc} is fully established, its exact form remains unknown and contains integrals of nonlocal quantities. It is therefore a challenging many-body problem to investigate this important quantity in real materials. In practical calculations, approximations to the energy functional E_{xc} are required. Commonly used ones include the local-density approximation (LDA), in which the density is assumed to be locally uniform and the result for a homogeneous electron gas is used point by point based on the local density, and the generalized gradient approximation (GGA), in which the gradient correction to the LDA is added.

In order to study systems of hundreds of atoms, one focuses on the properties of the valence electrons and employ norm-conserving pseudopotentials to model the effects of core electrons. The one-particle orbitals will be expanded in terms of plane waves to eliminate

any bias in the basis functions. The self-consistent solution of the corresponding Kohn-Sham orbitals will be carried out by evaluating relevant quantities in either the real space or momentum space.

We have performed first-principles calculations for various graphane structures. The structure and electronic properties of all conformations were investigated using first-principles density-functional calculations. Perdew-Burke-Ernzerhof parametrization Perdew et al. (1996) of the generalized gradient approximation were used in all the calculations. A kinetic energy cutoff of 280 eV in the plane-wave basis and appropriate Monkhorst-Pack k -points ($6 \times 6 \times 1$ for graphane and $10 \times 1 \times 1$ for graphane nanoribbons) were sufficient to converge the grid integration of the charge density. Although the first-principles approach systematically underestimates the band gaps Yang et al. (2008), we are interested primarily in the general feature of the conformations or membranes. The initial search for stable structures was carried out through classical molecular dynamics by means of Tersoff potential Tersoff (1988). The obtained local energy-minimum structures were further optimized through first-principles calculations with forces less than 0.01 eV/\AA .

The structural and electronic properties were investigated using first-principles density-functional calculations DMol₃ (2010). Our first-principles calculations are based on spin-polarized density functional theory with local density approximation (LDA) for exchange-correlation potential Vosko et al. (1980). A supercell with a vacuum space of 16 \AA normal to graphene plane was used. A kinetic energy change of $3 \times 10^{-4} \text{ eV}$ in the orbital basis and appropriate Monkhorst-Pack k -point grids of $6 \times 6 \times 1$ were sufficient to converge the integration of the charge density. The optimization of atomic positions proceeds until the change in energy is less than $1 \times 10^{-6} \text{ eV}$ per cell. Although the LDA approach systematically underestimates the band gaps, we are primarily interested in the relative stability of the conformations and the electric field effects. While calculations based on hybrid functionals or many-body GW approaches can rectify the gaps (the rectified gap is $5.2\text{--}5.4 \text{ eV}$ vs. the LDA result of 3.6 eV for graphane) Samarakoon & Wang (2009); Zhang et al. (2009), the implementation of the corresponding electric-field effect is cumbersome. The LDA approach is expected to provide qualitatively correct pictures and remains the popular choice for investigations of electric-field effects Zhang et al. (2009). Another reason for choosing LDA is attributed to the fact that generalized-gradient-approximation (GGA) leads to weak bonding between graphene layers and yields excessively large values of bilayer distance. By contrast, LDA calculation gives rise to a bilayer distance of $\sim 3.3 \text{ \AA}$ in good conformity with the results of graphite Partoens & Peeters (2006).

3. Results and discussion

3.1 Cyclohexane membranes

In order to effectively search for stable crystal structures of graphane, it is instructive to make reference to distinctive configurations of cyclohexane (see top panel of Figure 1) referred to as chair, boat, twist-boat and chair-twist-boat, respectively. Due to the inherent tendency of the sp^3 hybridization on tetravalent carbons, cyclohexane does not form a planar hexagonal arrangement. The chair isomer is the ground state configuration, while twist-boat is the second lowest-energy isomer. The chair conformation changes in the ring-flipping process, leading to the axial hydrogens becoming equatorial. Between the two stable chair states (with D_{3d} symmetry), the twist-boat (with D_2 symmetry), boat (with C_{2v} symmetry), and chair-twist-boat isomers can be constructed. The boat and chair-twist-boat forms are metastable states of the twist and chair forms, respectively. The twist-boat form

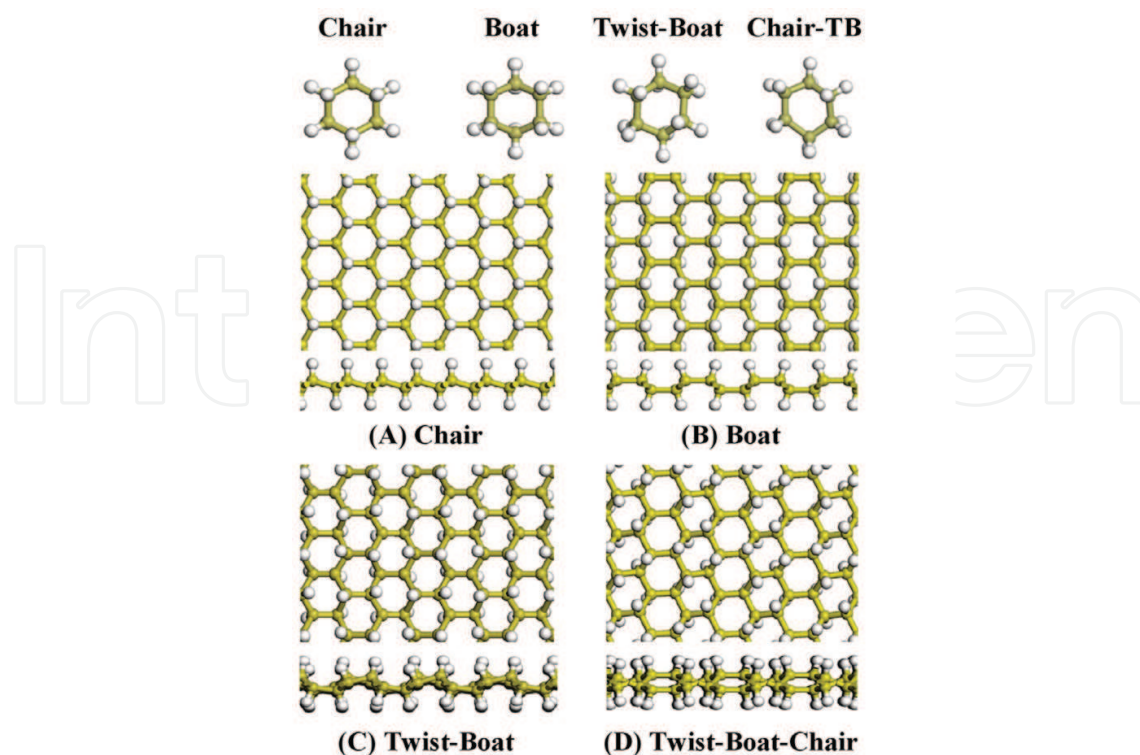


Fig. 1. Top panel: top view of chair, boat, twist-boat, and chair-twist-boat conformations of cyclohexane. Carbon atoms are shown as gold and hydrogen atoms are white. Middle and bottom panels: top and side views of graphane conformations for (A) chair, (B) boat, (C) twist-boat, and (D) twist-boat-chair, respectively. Reprinted with permission from Ref. Samarakoon & Wang (2009), Copyright © 2009 American Chemistry Society.

may be isolable because—like the chair form—it stands for an energy minimum. The boat conformation is free from angle strain, but has a higher energy than the chair form due to steric strain in connection to the flagpole interaction. The torsional strain in the boat conformation has a maximum value since two of the carbon bonds are fully eclipsed. This is to be contrasted to the chair conformer in which all bonds are staggered and complete absence of torsional strain, while the twist-boat has four partially eclipsed bonds.

3.2 Chair, boat, and twist-boat conformations in graphane

The counterparts of chair, boat, and twist-boat conformers of cyclohexane in two-dimensional structures of graphane can be constructed accordingly. We illustrate in Figure 1 the structures of chair, boat, and twist-boat conformations of graphane, along with a twist-boat-chair structure. The chair and boat structures coincide with configurations previously obtained using density functional calculations Boukhvalov et al. (2008); Sofo et al. (2007). The unit cell of chair and boat conformation has $P\bar{3}m1$ and $Pmmn$ symmetry, respectively. Consistent with the energy order of cyclohexane, the chair configuration is lower in energy and has less membrane buckling than those of boat conformer.

The twist-boat configuration of graphane has more in-plane shrinkage than either chair or boat conformation. However, the twist-boat structure becomes not stable against the boat conformation in geometry optimization using first-principles calculations. Closer scrutiny of the geometry optimization process from a twist-boat structure of graphane to the boat configuration reveals that the additional energy cost is attributed to the fact that all carbon

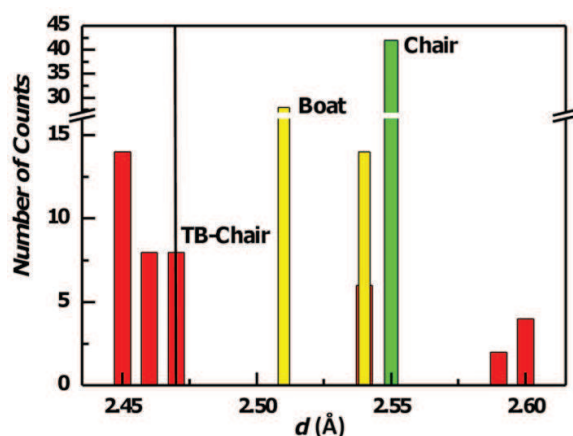


Fig. 2. The number of counts (collected from a sample with 42 lattice spacings) of in-plane lattice spacing for chair (green), boat (yellow), and twist-boat-chair (red) conformations of graphene, respectively. The vertical solid line corresponds to theoretical in-plane lattice spacing of graphene. Reprinted with permission from Ref. Samarakoon & Wang (2009), Copyright © 2009 American Chemistry Society.

Structure	E_B (eV)	E_g (eV)	a (Å)	a_0 (Å)	d (Å)
Graphene	-8.57	0	1.42	1.42	2.47
Chair	-12.23	3.5	1.54	1.47	2.55
Boat	-12.06	3.5	1.54, 1.58	1.40, 1.58	2.51, 2.54
TB-Chair	-11.97	3.8	1.53-1.57	0.89-1.51	2.45-2.60

Table 1. Calculated binding energy per carbon atom E_B , band gap E_g , the bond length a and the associated planar projection a_0 , the in plane lattice spacing d for chair, boat, twist-boat(TB)-chair conformations of graphene, respectively. Reprinted with permission from Ref. Samarakoon & Wang (2009), Copyright © 2009 American Chemistry Society.

atoms in the unit cell participate in the bond twisting process. By contrast, in cyclohexane only four out of six carbon atoms mimicking a pair of twist bonds are involved in the optimization between boat and twist-boat forms.

3.3 Lattice contraction in graphene

It becomes clear that the experimentally observed graphene is unlikely to be in the single crystal form of chair, boat, or twist-boat, since each of those structures has only one or two distinctive in-plane lattice spacing, in contrast to a wide range of distribution observed experimentally Elias et al. (2009). Moreover, the twist-boat configuration is no longer stable against the boat structure. However, the instability of the twist-boat crystal structure does not preclude the existence of locally stable twist-boat membranes. To pursue this scenario, we show in Figure 1 a twist-boat-chair configuration, which consists of adjacent twist-boat and chair membranes. Our first-principles calculation shows that the twist-boat-chair configuration is a stable structure of graphene, although the energy is slightly higher than the boat and chair conformations. Summarized in Table I are the structural and electronic properties of the conformation as compared to those for graphene as well as chair and boat conformations of graphene. It is worth noting that in the twist-boat-chair configuration, locally stable twist-boat membranes are favored over boat ones since two carbon atoms in the membrane serve as linkage atoms for the neighbor chair membranes. The unit cell of twist-boat-chair structure has a P_2/c symmetry with monoclinic angle $\gamma = 138.5^\circ$.

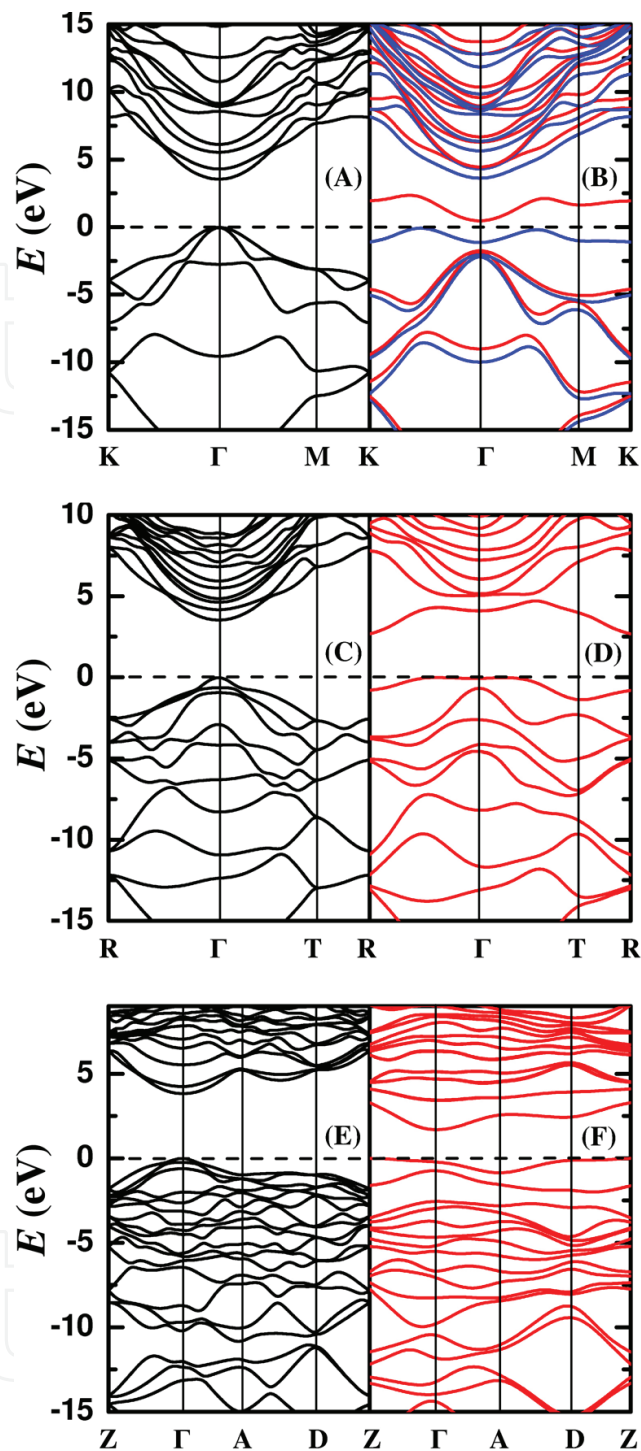


Fig. 3. Calculated band structure for (A) chair, (C) boat, and (E) twist-boat-chair conformations of graphane, and their counterparts (B), (D), and (F) for one-side half-hydrogenated graphane (graphone), respectively. The red and blue curves represent spin-up and spin-down components, respectively. For chair conformation, $\mathbf{K}=(\pi/3a, 2\pi/3a)$, $\mathbf{M}=(0, \pi/2a)$, where $a = 2.55 \text{ \AA}$. For boat conformation, $\mathbf{R}=(\pi/2b_1, \pi/2b_2)$, $\mathbf{T}=(\pi/2b_1, 0)$, where $b_1 = 2.55 \text{ \AA}$ and $b_2 = 4.33 \text{ \AA}$. For twist-boat-chair conformation, $\mathbf{Z}=(0, \pi/2c_2)$, $\mathbf{A}=(\pi/2c_1, 0)$, $\mathbf{D}=(\pi/2c_1, \pi/2c_2)$, where $c_1 = 6.63 \text{ \AA}$ and $c_2 = 4.92 \text{ \AA}$. The valence band maximum is set to 0 eV. Reprinted with permission from Ref. Samarakoon & Wang (2009), Copyright © 2009 American Chemistry Society.

An important ramification of our investigation of various graphane crystal structures is that the low energy conformations have no more than one parallel aligned nearest neighbor hydrogens, as the hydrogen in chair and boat has zero and one parallel aligned neighbor, respectively. On the other hand, the chair membranes in the twist-boat-chair structure may have two neighboring hydrogens. This trend is also observable for various other stable structures of graphane. We depict in Figure 2 the distribution of lattice spacing for various crystal structures of graphane. For the chair conformation, there exists only one distinctive lattice spacing. For the boat conformer, there are two distinctive in-plane lattice spacings. The twist-boat-chair conformation has a broad range of in-plane lattice spacings from 2.45–2.60 Å. The lowest lattice spacing of 2.45 Å is about 1% of lattice contraction as compared with the value obtained for graphene (2.47 Å), which is about 5% contraction of the value for chair (2.55 Å). This contraction can be correlated to short in-plane bond lengths which can be as small as 0.89 Å (see Table 1).

The transformation among various graphane structures amounts to flipping hydrogens from one side of the plane to another, along with the associated strain relaxation for the carbon atoms attached. The transition states are characterized with distortions of the hexagonal network with elongated carbon bonds in order to accommodate hydrogens that are in the network plane during the flipping process. This implies that once the hydrogens are absorbed onto graphene with fully saturation, it becomes difficult for the system to adopt the ground-state chair conformation. As a result, the sequence of alternating hydrogens on both sides of the plane is broken, introducing other type of membranes into the crystal structure of graphane. Consequently, this leads to out of plane distortions that induce in-plane shrinkage and results in a decrease of the in-plane lattice spacing in relation to that of the chair conformation.

We believe that the experimentally observed broad distribution of lattice spacings can be attributed, to a large extent, to the existence of membranes other than the chair form. In this regard, locally stable twist-boat membrane, as exemplified in twist-boat-chair, is the prototype of low energy configurations with paralleled aligned nearest-neighbor hydrogens. Furthermore, as exemplified in the twist-boat-chair structure, the twist-boat conformer serves as effective link to neighboring chair conformers.

3.4 Electronic band structures

The band gap of the twist-boat-chair structure, together with that of the chair and boat conformations can be extracted from the corresponding band structures illustrated in Figure 3. The band structure for twist-boat-chair resembles an interpolation of those of chair and boat ones, and the corresponding band gap of 3.8 eV is very close to those obtained for chair and boat structures Boukhvalov et al. (2008); Sofo et al. (2007). In all the cases, the graphane structures have direct gaps at the band center (Γ point).

3.5 Graphone

Recently, structures with one-sided hydrogenation that are reminiscent of hydrogenation on epitaxial graphene Guisinger et al. (2009) or graphene on a substrate have attracted a great deal of attention Elias et al. (2009). Of particular interest is the recent theoretical prediction that semi-hydrogenated graphene (graphone) becomes a ferromagnetic semiconductor with a small indirect gap. Zhou et al. (2009) The half-hydrogenation in the chair conformation breaks the delocalized π bonding network of graphene, leaving the electrons in the unhydrogenated carbon atoms localized and unpaired. While the idea of a ferromagnetic semiconducting graphone is extremely provocative, a careful examination of various graphone configurations

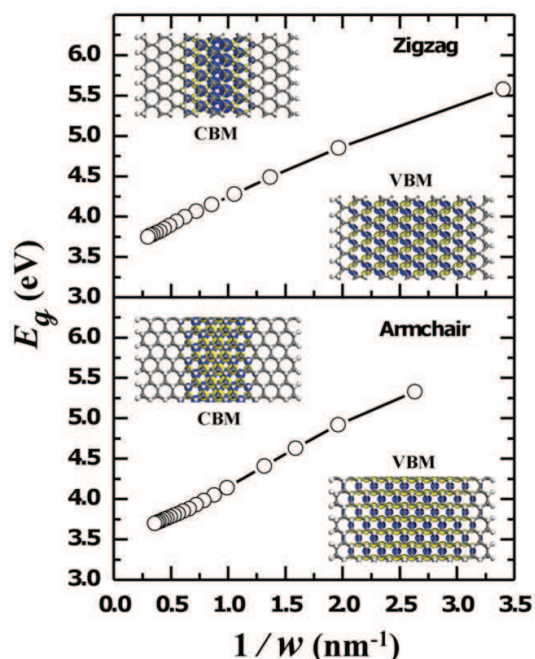


Fig. 4. Calculated band gaps of nanoribbons of graphane with zigzag (top panel) and armchair (bottom panel) edges, respectively. Insets: extracted charge density distribution at the band center (Γ point) of the corresponding CBM and VBM states, respectively. Reprinted with permission from Ref. Samarakoon & Wang (2009), Copyright © 2009 American Chemistry Society.

is necessary. Our calculation of the chair, boat, and twist-boat-chair conformations of graphane reveals that the ferromagnetic state with an indirect gap of 0.51 eV (see Figure 3B) is very fragile. An implication is that spin-polarized valence band maximum states show long-range correlations and thus depend on the size of the unit cell studied. On the other hand, the ground state of boat and twist-boat-chair conformations is nonmagnetic (Figures 3D and 3F). Moreover, in contrast to graphane in that the chair configuration is the lowest energy configuration, the energy for boat-graphane of -9.88 eV is lower than that of -9.42 eV for chair-graphane.

3.6 Graphane nanoribbons

The reason for a band gap opening up in hydrogenated graphene can be attributed to the changes from sp^2 bonded C atoms to sp^3 bonded ones Sofo et al. (2007). We have found that all the fully saturated graphane structures have a wide gap, including graphane nanoribbons. Shown in Figure 4 is the dependence of band gaps on the width of the graphane nanoribbon with armchair and zigzag edges. The naming of the armchair and zigzag nanoribbons follows the edge structure nomenclature, such that an armchair (zigzag) tube unfolds into a zigzag (armchair) ribbon Baron et al. (2006); Son et al. (2006). The ribbons involved in the present study were constructed based on chair conformations and were neutral bond saturated with hydrogen passivation at edges.

As is readily observable in Figure 4, the gaps of the ribbon decrease with increasing width w in an approximate $1/w$ fashion. The extracted charge density distribution of the conduction band minimum (CBM) and valence band maximum (VBM), as seen from insets of Figure 4, indicates predominantly confined electrons and holes in the proximity of ribbon center. The

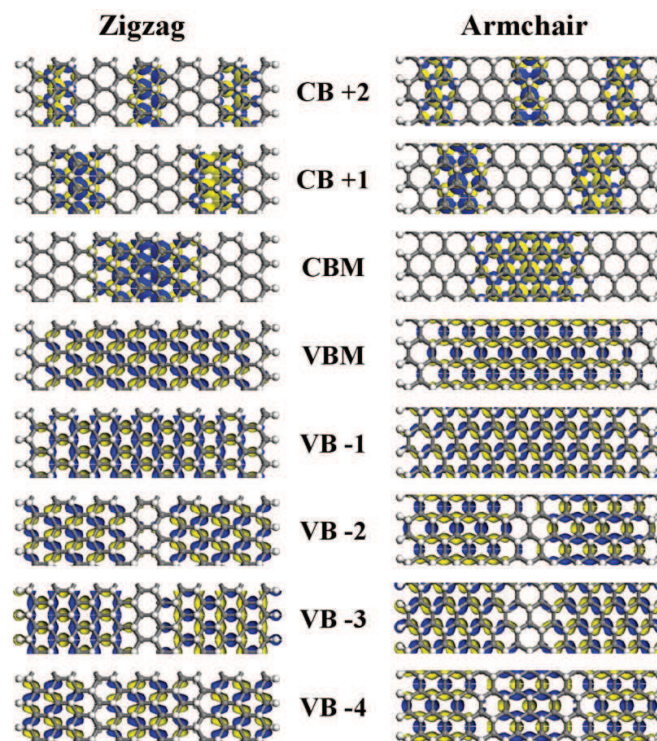


Fig. 5. Charge density distributions of near gap conduction and valence states for armchair (left panels) and zigzag (right panels) edged graphane nanoribbons, respectively. The sign of the wave function is indicated by light blue and yellow regions, respectively. The isovalue is 0.025 au. Reprinted with permission from Ref. Samarakoon & Wang (2009), Copyright © 2009 American Chemistry Society.

calculated gaps are insensitive to the details of the ribbon edge geometry and termination, in sharp contrast to sp^2 bonded graphene nanoribbons (GNRs). The band gap of ultra-thin GNR with armchair edges generally opens up due to the quantum confinement and the edge bond relaxation. The oscillatory band gap for GNR with armchair edges can be explained by the Fermi wavelength in the direction normal to the ribbon direction Baron et al. (2006); Son et al. (2006). Similar to zigzag SWNTs, the band gaps of AGNRs are divided into three groups, with the $3p + 2$, $3p + 1$, and $3p$ group (p is a positive integer) having a small, medium, and large gap, respectively Baron et al. (2006); Son et al. (2006). It is worth noting that the oscillatory behavior of sp^2 bonded GNRs completely disappears for sp^3 bonded graphane nanoribbons Li et al. (2009). Furthermore, our calculations based on spin-polarized calculations confirmed that the ground state of graphane nanoribbons with zigzag edges is not magnetic, in contrast to the staggered antiferromagnetic state for zigzag GNRs Son et al. (2006).

The extracted density distribution of holes and electrons for graphane nanoribbons with zigzag and armchair edges is illustrated in Figure 5. For conduction bands, the near gap states exhibit s , p , d , ... characters, in conformity with predictions from one-dimensional particle-in-a-box model Nduwimana et al. (2008). The s , p , d , ... features are also observable for valence states, but for a pair of nearly degenerate (at the band center) valence bands. The close resemblance of the charge distributions for zigzag and armchair edged graphane nanoribbons indicates that edge effect becomes dormant for sp^3 bonded ribbons. These results suggest that by tailoring the effective ribbon width it is feasible to design semiconductor graphane nanoribbons with a tunable band gap, which is advantageous over GNRs in that one can

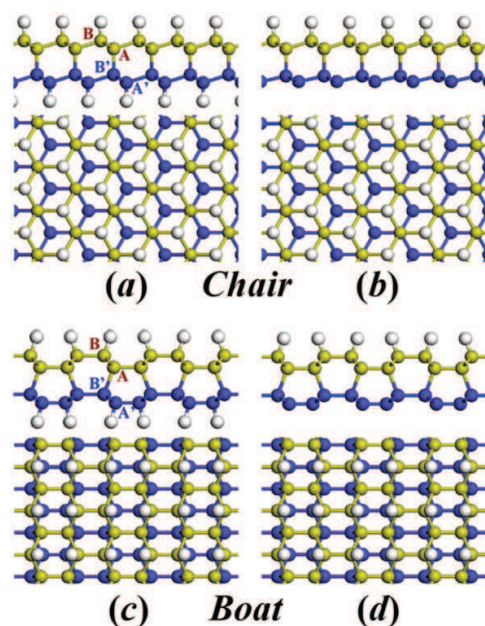


Fig. 6. Top panel: top and side views of (a) fully hydrogenated and (b) semi-hydrogenated chair conformations of bilayer graphene. Bottom panels: top and side views of (c) fully hydrogenated and (d) semi-hydrogenated boat structures of bilayer graphene. Carbon atoms on top and on bottom layers are colored with gold and blue, respectively. Hydrogen atoms are colored with white. Reprinted with permission from Ref. Samarakoon & Wang (2009), Copyright © 2009 American Chemistry Society.

avoid the daunting task of identifying the edge structures. Accordingly, the control of proper nanostructures may offer avenues for the design of highly effective nanodevices.

3.7 Patterned hydrogenation

The approach described in the present work can be employed to investigate hydrogenated graphene systems, such as patterned graphene nanoroads Singh & Yakobson (2009) that are composed of GNRs with fully saturated hydrogenation at the edges and well-defined sharp interfaces between sp^2 and sp^3 bonded membranes. Of particular interest is the interplay between sp^2 and sp^3 hybridizations that can be systematically investigated via band alignment analysis. The band alignment for patterned graphene nanoroads is based on the lineup of charge neutrality levels Nduwimana & Wang (2009) for sp^2 and sp^3 bonded components. Since sp^3 hybridization leads to wide gap semiconducting behavior, the electronic properties of patterned nanoroads are primarily determined by the sp^2 components. For instance, for graphene nanoroads with armchair edges, the band gaps are in accordance with results of GNRs with the effective sp^2 width and show oscillatory behavior Singh & Yakobson (2009).

3.8 Bilayer graphane

While the opening and external tuning of energy gap between valence and conduction bands in Bernal stacking bilayer graphene McCann (2006); Ohta et al. (2006) hold great potential for logic applications, switching off the conduction to a desirable level remains challenging in epitaxial graphene Neto et al. (2009). In this regard, it is of interest to investigate bilayer hydrogenated graphene that is semiconducting from the onset. Figure 6 depicts the fully and half hydrogenated chair and boat conformations. As can be seen from Figure 6, for the

Structure	E_B (eV)	E_g (eV)	l (Å)
Fully-hydrogenated Chair	-12.00	3.24	1.54
Fully-hydrogenated Boat	-11.93	2.92	1.54
Semi-hydrogenated Chair	-10.55	0.54	1.65
Semi-hydrogenated Boat I	-10.79	2.35	1.63
Semi-hydrogenated Boat II	-10.85	0.50	3.26

Table 2. Calculated binding energy per carbon atom E_B , band gap E_g , and the inter-layer bond length l for chair and boat conformations of fully hydrogenated and semi-hydrogenated graphene, respectively. Label I and II refers to boat conformations with and without interlayer bonding, respectively. Reprinted with permission from Ref. Samarakoon & Wang (2010), Copyright © 2009 American Chemistry Society.

fully-hydrogenated structures a chemical bonding between the $A - B'$ sites stabilizes both chair and boat conformations. In the latter case, the chemical bonding induces a structural transformation that deviates from the pattern of Bernal stacking.

3.9 Structural properties of bilayer graphane

The geometry details are listed in Table 2 along with the calculated binding energy and band gap. Analogous to graphane from the one-layer fully-hydrogenated graphene, the chair conformation Flores et al. (2009); Samarakoon & Wang (2009) is the lowest energy conformation for fully hydrogenated bilayer, in agreement with previous first-principles density-functional predictions Sofo et al. (2007). Furthermore, the corresponding chemical bonding between the bilayer remains stable with the desorption of hydrogen in one layer, resulting in a slight increase of the inter-layer bonding distance from 1.54 Å to 1.65 Å (Table 2). It is important to remark that while the inter-layer chemical bonding remains intact after desorption of hydrogens in one layer, the lowest energy configuration for one-sided hydrogenation is a boat conformation without the chemical bonding (Table 2). The crucial difference between the hydrogen desorption in one layer and the one-sided hydrogenation should be of particular interest in the forthcoming discussions.

3.10 Electronic properties of bilayer graphane under electric bias

There have been a number of theoretical studies on opening up a band gap in the gapless bilayer graphene if an electric field is applied perpendicularly Avetisyan et al. (2009); Grüneis et al. (2008); Liu & Shen (2009). The effect of the electric field can be studied by adding a potential *via* the nuclear charges. Our calculations show that the bilayer graphene opens a gap of ~ 0.23 eV by an electric bias of ~ 0.51 V/Å. This is in agreement with other theoretical predictions and experimental observations Avetisyan et al. (2009); Zhang et al. (2009). However, when the electric bias is further increased, the gap in the bilayer system collapses, and the system turns back to metallic with induced interlayer bonding $A - B'$ reminiscent of the hydrogenated bilayer graphene. We show in Figure 7 the calculated band structures for bilayer graphane for chair conformation. As is readily observable from Figure 7, the band gap decreases monotonically from about 3.24 to 0 eV with increase of electric bias. The critical bias for the semiconducting to metallic transition is estimated to be 1.05 V/Å. Shown in Figure 8 are the corresponding charge densities. In the absence of bias, the charge density distributions are symmetrical both in conduction and valence bands. With the application of an electric bias, charges transfer in the conduction and valence bands acts in

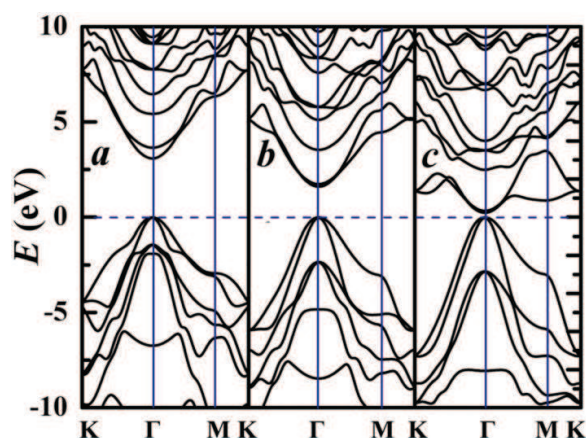


Fig. 7. Calculated band structure of fully-hydrogenated graphene in chair conformation with (a) no electric bias, (b) $0.39 \text{ V}/\text{\AA}$ electric bias, and (c) $1.03 \text{ V}/\text{\AA}$ electric bias, respectively. $K = (\pi/3a, 2\pi/3a)$, $M = (0, \pi/2a)$, where $a = 2.50 \text{ \AA}$. The valence band maximum is set to 0 eV. Reprinted with permission from Ref. Samarakoon & Wang (2010), Copyright © 2009 American Chemistry Society.

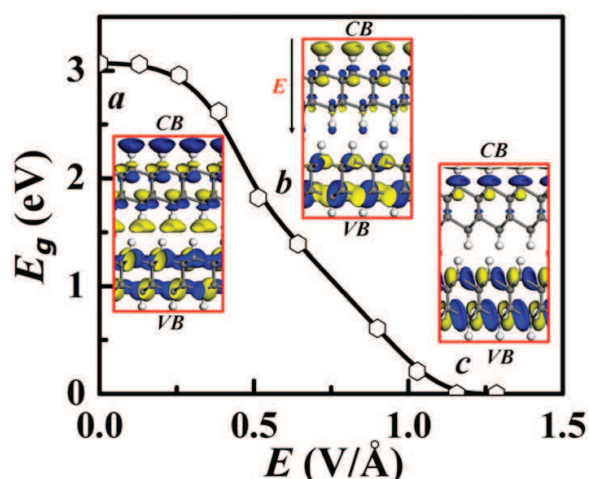


Fig. 8. Calculated dependence of band gap on perpendicular applied electric bias for the bilayer graphene in chair conformation: (a) no bias, (b) $0.39 \text{ V}/\text{\AA}$ electric bias, and (c) $1.03 \text{ V}/\text{\AA}$ electric bias, respectively. Insets: extracted charge density distribution at the band center (Γ point) of the corresponding conduction and valence band states. The isovalue is 0.025 au. Reprinted with permission from Ref. Samarakoon & Wang (2010), Copyright © 2009 American Chemistry Society.

a concerted fashion, resulting in charge accumulation and depletion in the conduction and valence bands, respectively.

3.11 Bilayer graphone

It is worth noting that there is no explicit magnetic states in fully-hydrogenated bilayer graphene. This indicates that the chemical bonds and the electric-field induced dipole-dipole interaction do not lead to unpaired spins. The unpaired spins can be generated through desorption of the hydrogen in one layer or through one-sided absorption. The latter scenario is particularly interesting in that one can take advantage of the electric field that generates chemical bonding prior to the hydrogenation. However, the chemical bonding is

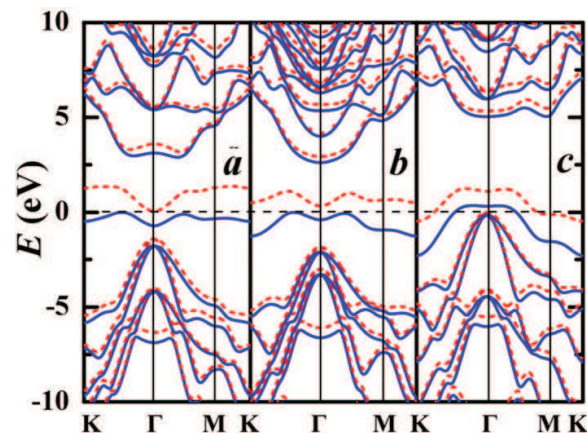


Fig. 9. Calculated band structure for semi-hydrogenated bilayer graphene in chair conformation with (a) -0.26 V/\AA electric bias, (b) no electric bias, and (c) 0.39 V/\AA electric bias, respectively. The red and blue curves represent spin-up and down components, respectively. Reprinted with permission from Ref. Samarakoon & Wang (2010), Copyright © 2009 American Chemistry Society.

simultaneously breaking when the electric bias is switched off. We have carefully studied both scenarios. The desorption of the fully-hydrogenated chair conformation can be readily confirmed. However, the one-sided hydrogenation is much more involved due to the crucial dependence of the hydrogenation patterns, which favors a boat conformation at large hydrogen coverage that is non-magnetic.

Hydrogenation of graphene is reversible, providing the flexibility to manipulate its coverage Elias et al. (2009). The desorption of the hydrogen atoms from one side of graphene will result in a semi-hydrogenated bilayer graphene which is the counterpart of the monolayer "graphone" Zhou et al. (2009). Graphone is a ferromagnetic semiconductor with a small indirect gap attributed to the breaking of the delocalized π -bonding network of graphene delocalization, which is associated with localized and unpaired electrons Boukhvalov et al. (2008); Zhou et al. (2009). Shown in Figure 9 are the calculated band structures for one side hydrogenated bilayer graphene under electric bias. For semi-hydrogenated bilayer graphene there is an indirect band gap about 0.54 eV (Figure 9b). This changes to metallic for biased voltages below -0.26 V/\AA (Figure 9a) or above 0.39 V/\AA (Figure 9c).

Our results show that the bilayer counterpart of graphone is ferromagnetic. Partial saturation of carbon atoms in hydrogenated graphene breaks its π -bonding network resulting in localized and unpaired electrons Zhou et al. (2009). The magnetic moments couple ferromagnetically with the semi-hydrogenated chair conformation. Electronic structure changes by partial hydrogenation as well. The semi-hydrogenated graphene of chair conformation is an indirect band gap semiconductor with a small band gap, very different from the original graphene and graphane. We illustrate in Figure 10 the dependence of the spin-polarized bands of semi-hydrogenated bilayer graphene with the positive and negative bias. The energy gap decreases monotonically with the electric field by characterizing the properties from magnetic semiconductor with a small gap, to a metal with a zero gap. In contrast to fully-hydrogenated bilayer graphene, the changes in the gap are no longer symmetrical with the negative and positive bias. Apart from the partial shifts of the spin density to the bottom layer, closer scrutiny reveals a paucity of modifications of the spin-density distribution, when the applied electric field goes from negative to positive bias. In connection to the spin density shift, the band dispersion changes from nearly flat to

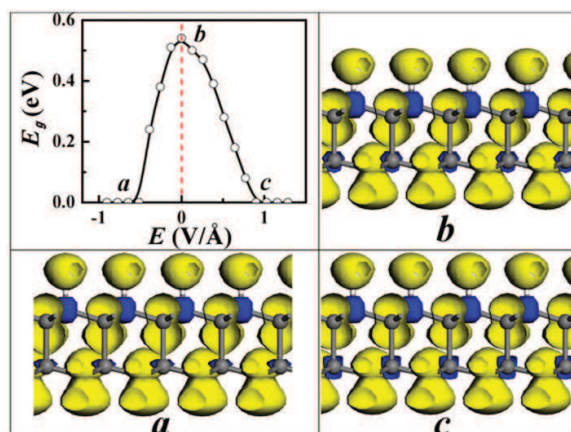


Fig. 10. Calculated band gaps of semi-hydrogenated bilayer graphene in chair structure with (a) -0.26 V/\AA electric bias, (b) no bias, and (c) 0.39 V/\AA electric bias, respectively. Insets: extracted spin density distribution at the band center (Γ point) of the corresponding conduction and valence states. The isovalue is 0.025 au . Reprinted with permission from Ref. Samarakoon & Wang (2010), Copyright © 2009 American Chemistry Society.

pronounced dispersion near the band edge at K , which leads to the change of the indirect gaps.

4. Conclusion

4.1 Chair, boat, and twist-boat membranes in graphane

We have studied various stable crystal structures of graphane and demonstrated that locally stable twist-boat membranes significantly contribute to the experimentally observed lattice contraction. The first-principles results shed considerable light on the electronic characteristics associated with the sp^3 hybridization. Moreover, the first-principles approach can be employed to structural and electronic properties of hydrogenated graphene derivatives. The understanding of structural and electronic stability thus provides a useful means for future development of graphane-based nanodevices.

4.2 Bilayer graphane under electric bias

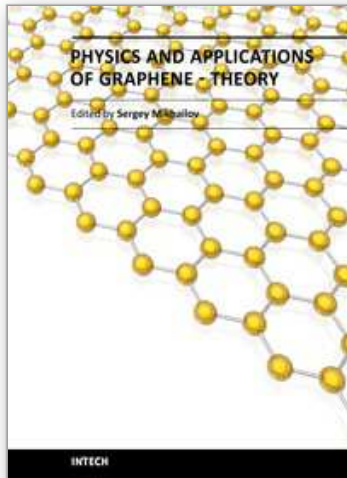
We have studied the electronic characteristics of biased bilayer graphane. The resultant hydrocarbon compound, bilayer graphane, can be modified into new materials, fine-tuning its electronic properties. These studies have revealed increasingly fertile possibilities in hydrogen storage and two-dimensional electronics. These novel semiconducting behaviors result from a peculiar, effective transformation of sp^2 to sp^3 carbon and allow a continuously tunable band gap in biased bilayer graphane. A bilayer version can deliver yet another interesting feature of tunable band gap. This discovery paves the way for new electronic devices, from lasers that change color to electronic circuits that can rearrange themselves. The tunable band gap, which generally determines transport and optical properties, will enable flexibility and optimization of graphane-based nanodevices. Moreover, our proposed desorption of hydrogen from one layer, coupled with controlled hydrogen-vacancy distribution and patterned hydrogenation, could provide a promising route to realize a ferromagnetic semiconductor in view of the crucial structural difference between monolayer graphane and the bilayer semi-hydrogenated graphane.

5. References

- a. Avetisyan, A. A.; Partoens, B.; Peeters, F. M. (2009). Electric Field Tuning of the Band Gap in Graphene Multilayers, *Phys. Rev. B* 79 (3): 035421 – 035427.
- b. Avetisyan, A. A.; Partoens, B.; Peeters, F. M. (2009). Electric-Field Control of the Band Gap and Fermi Energy in Graphene Multilayers by Top and Back Gates, *Phys. Rev. B* 80 (19): 195401 – 195421.
- Barone, V.; Hod, O.; Scuseria, G. E. (2006). Electronic Structure and Stability of Semiconducting Graphene Nanoribbons, *Nano. Lett.* 6 (12): 2748 – 2754.
- Berger, C.; Song, Z.; Li, X.; Wu, X.; Brown, N.; Naud, C.; Mayou, D.; Li, T.; Hass, J.; Marchenkov, A. N.; Conrad, E. H.; First, P. N.; de Heer, W. A. (2006). Electronic Confinement and Coherence in Patterned Epitaxial Graphene, *Science* 312 (5777): 1191 – 1196.
- Boukhvalov, D. W.; Katsnelson, M. I.; Lichtenstein, A. I. (2008). Hydrogen on graphene: Electronic Structure, Total Energy, Structural Distortions and Magnetism from First-Principles Calculations, *Phys. Rev. B* 77 (3): 035427 – 035433.
- Castro, E. V.; Novoselov, K. S.; Morozov, S. V.; Peres, N. M. R.; dos Santos, J. M. B. L.; Nilsson, J.; Guinea, F.; Geim, A. K.; Neto, A. H. C. (2007). Biased Bilayer Graphene: Semiconductor with a Gap Tunable by the Electric Field Effect, *Phys. Rev. Lett.* 99 (21): 216802-216805f.
- Castro, E. V.; Peres, N. M. R.; dos Santos, J. M. B. L.; Guinea, F.; Neto, A. H. C. (2008). Bilayer Graphene: Gap Tunability and Edge Properties, *J. Phys.: Conf. Ser.* 129 (1): 012002.
- Ciftja, O. & Fantoni, S. (1996). A New Hypernetted-Chain Treatment for Laughlin Quantum Hall States, *Europhys. Lett.* 36 (9): 663 – 667.
- Ciftja, O. (2000). The Fermi-Sea-Like Limit of the Composite Fermion Wave Function, *Eur. Phys. J. B* 13 (4): 671 – 677.
- Ciftja, O. & Wexler, C. (2001). Energy Gaps for Fractional Quantum Hall States Described by a Chern-Simons Composite Fermion Wavefunction, *Eur. Phys. J. B* 23 (4): 437 – 440.
- DMol3 (2010). Accelrys Software Inc., San Diego, CA.
- Elias, D. C.; Nair, R. R.; Mohiuddin, T. M. G.; Morozov, S. V.; Blake, P.; Halsall, M. P.; Ferrari, A. C.; Boukhvalov, D. W.; Katsnelson, M. I.; Geim, A. K.; Novoselov, K. S. (2009). Control of Graphene's Properties by Reversible Hydrogenation: Evidence for Graphane, *Science* 323 (5914): 610 – 613.
- Flores, M. Z. S.; Autreto, P. A. S.; Legoas, S. B.; Galvao, D. S. (2009). Graphene to Graphane: a Theoretical Study, *Nanotechnology* 20 (46): 465704 – 465709.
- a. Geim, A. K. & Novoselov, K. S. (2007). The Rise of Graphene, *Nature Mater.* 6: 183 – 191.
- b. Geim, A. K.; Morozov, S.V.; Hill, E. W.; Blake, P.; Katsnelson, M. I.; Novoselov, K. S. (2007). Detection of Individual Gas Molecules Adsorbed on Graphene, *Nat. Mater.* 6: 652 – 655 .
- Gilje, S.; Han, S.; Wang, M., Wang, K. L.; Kaner, R. B. (2007). A Chemical Route to Graphene for Device Applications, *Nano Lett.* 7 (11): 3394 – 3398.
- Giovannetti, G.; Khomyakov, P. A.; Brocks, G.; Kelly, P. J.; van den Brink, J. (2007). Substrate-Induced Band Gap in Graphene on Hexagonal Boron Nitride: *Ab Initio* Density Functional Calculations, *Phys. Rev. B* 76 (7): 073103 – 073106.
- Guisinger, N. P.; Rutter, G. M.; Crain, J. N.; First, P. N.; Stroscio, J. A. (2009). Exposure of Epitaxial Graphene on SiC(0001) to Atomic Hydrogen, *Nano Lett.* 9 (4): 1462 – 1466.
- Grüneis, A.; Attacalite, C.; Wirtz, L.; Shiozawa, H.; Saito, R.; Pichler, T.; Rubio, A. (2008). Tight-Binding Description of the Quasiparticle Dispersion of Graphite and Few-Layer Graphene, *Phys. Rev. B* 78 (20): 205425 – 205440.

- Halperin, B.; Lee, P. A.; Read, N. (1993). Theory of the Half-Filled Landau Level, *Phys. Rev. B* 47 (12): 7312 – 7343.
- Jain, J. K. (1989). Composite-Fermion Approach for the Fractional Quantum Hall Effect, *Phys. Rev. Lett.* 63 (2): 199-202.
- Kresse, G. & Furthmuller, J. (1996). Efficient Iterative Schemes for *Ab Initio* Total-energy Calculations Using a Plane-wave Basis Set, *Phys. Rev. B* 54 (16): 11169 – 11186.
- Laughlin, R. B. (1983). Anomalous Quantum Hall Effect: An Incompressible Quantum Fluid with Fractionally Charged Excitations, *Phys. Rev. Lett.* 50 (18): 1395 – 1398.
- Leenaerts, O.; Partoens, B.; Peeters, F. M. (2009). Hydrogenation of Bilayer Graphene and the Formation of Bilayer Graphane from First Principles, *Phys. Rev. B* 80 (24): 245422 – 245427 .
- Li, X.; Wang, X.; Zhang, L.; Lee, S.; Dai, H. (2008). Chemically Derived, Ultrasoft Graphene Nanoribbon Semiconductors, *Science* 319 (5867): 1229 – 1232.
- Li, Y.; Zhou, Z.; Shen, P.; Chen, Z. (2009). Structural and Electronic Properties of Graphane Nanoribbons, *J. Phys. Chem. C* 113 (33): 15043 – 15045.
- Liu, L. & Shen, Z. (2009). Bandgap Engineering of Graphene: A Density Functional Theory Study, *Appl. Phys. Lett.* 95 (25): 252104 – 252107.
- Mak, K. F.; Lui, C. H.; Shan, J.; Heinz, T. F. (2009). Observation of an Electric-Field-Induced Band Gap in Bilayer Graphene by Infrared Spectroscopy, *Phys. Rev. Lett.* 102 (25): 256405 – 256408.
- McCann, E. (2006). Asymmetry Gap in the Electronic Band Structure of Bilayer Graphene, *Phys. Rev. B* 74 (16): 161403 – 161406.
- Min, H.; Sahu, B.; Banerjee, S. K.; MacDonald, A. H. (2007). *Ab Initio* Theory of Gate Induced Gaps in Graphene Bilayers, *Phys. Rev. B* 75 (15): 155115 – 155121.
- Nduwimana, A.; Musin, R. N.; Smith, A. H.; Wang, X.-Q. (2008). Spatial Carrier Confinement in Core-Shell and Multishell Nanowire Heterostructures, *Nano Lett.* 8 (10): 3341 – 3344.
- Nduwimana, A. & Wang, X.-Q. (2009). Charge Carrier Separation in Modulation Doped Coaxial Semiconductor Nanowires, *Nano Lett.* 9 (1): 283 – 286.
- Nduwimana, A. & Wang, X.-Q. (2009). Energy Gaps in Supramolecular Functionalized Graphene Nanoribbons, *ACS Nano* 3 (7): 1995 – 1999.
- Neto, A. H. C.; Guinea, F.; Peres, N. M. R.; Novoselov, K. S.; Geim, A. K. (2009). The Electronic Properties of Graphene, *Rev. Mod. Phys.* 81: 109 – 162.
- Nilsson, J.; Neto, A. H. C.; Guinea, F.; Peres, N. M. R. (2008). Electronic Properties of Bilayer and Multilayer Graphene, *Phys. Rev. B* 78(4): 045405 – 045438.
- Novoselov, K. S.; Geim, A. K.; Morozov, S. V.; Jiang, D.; Zhang, Y.; Dubonos, S. V.; Grigorieva, I. V.; Firsov, A. A. (2004). Electric Field Effect in Atomically Thin Carbon Films, *Science* 306 (5696): 666 – 669.
- Novoselov, K. S.; Geim A. K.; Morozov, S. V.; Jiang, D.; Katsnelson, M. I.; Grigorieva, I. V.; Dubonos, S. V.; Firsov, A. A. (2005). Two-dimensional Gas of Massless Dirac Fermions in Graphene, *Nature* 438: 197-200.
- Ohta, T.; Bostwick, A.; Seyller, T.; Horn, K.; Rotenberg, E. (2006). Controlling the Electronic Structure of Bilayer Graphene, *Science* 313 (5789): 951 – 954.
- Oostinga, J. B.; Heersche, H. B.; Liu, X.; Morpurgo, A. F.; Vandersypen, L. M. (2008). Gate-Induced Insulating State in Bilayer Graphene Devices, *Nat. Mater.* 7 : 151- 157.
- Partoens, B. & Peeters, F. M. (2006). From Graphene to Graphite: Electronic Structure Around the K Point, *Phys. Rev. B* 74 (7): 075404 – 075414.

- Perdew, J. P.; Burke, K.; Ernzerhof, M. (1996). Generalized Gradient Approximation Made Simple, *Phys. Rev. Lett.* 77 (18): 3865 – 3868.
- Samarakoon, D. K. & Wang, X.-Q. (2009). Chair and Twisted-Boat Membranes in Hydrogenated Graphene, *ACS Nano* 3 (12): 4017 – 4022.
- Samarakoon, D. K. & Wang, X.-Q. (2010). Tunable Band Gap in Hydrogenated Bilayer Graphene, *ACS Nano* 4 (7): 4126 – 4130.
- Singh, A. K. & Yakobson, B. I. (2009). Electronics and Magnetism of Patterned Graphene Nanoroads, *Nano Lett.* 9 (4): 1540 – 1543.
- Sofa, J. O.; Chaudhari, A. S.; Barber, G. D. (2007). Graphane: A Two-Dimensional Hydrocarbon, *Phys. Rev. B* 75 (15): 153401 – 153404.
- Son, Y.-W.; Cohen M. L.; Louie, S. G. (2006). Energy Gaps in Graphene Nanoribbons, *Phys. Rev. Lett.* 97 (21): 216803 – 216806.
- Terstoff, J. (1988). New Empirical Approach for the Structure and Energy of Covalent Systems, *Phys. Rev. B* 37(12): 6991 – 7000.
- Thouless, D. J. (1998). *Topological Quantum Numbers in Nonrelativistic Physics*, World Scientific, Singapore.
- Tsui, D. C.; Stormer, H. L.; Gossard, A. C. (1982). Two-Dimensional Magnetotransport in the Extreme Quantum Limit, *Phys. Rev. Lett.* 48 (22): 1559 – 1562.
- Vosko, S. H.; Wilk, L.; Nusair, M. (1980). Accurate Spin-Dependent Electron Liquid Correlation Energies for Local Spin Density Calculations: a Critical Analysis, *Can. J. Phys.* 58 (8): 1200 – 1211.
- Wang, X.; Zhi, L.; Mullen, K. (2008). Transparent, Conductive Graphene Electrodes for Dye-Sensitized Solar Cells, *Nano Lett.* 8 (1): 323 – 327.
- Wen, X. G. (1990). Electrodynamical Properties of Gapless Edge Excitations in the Fractional Quantum Hall States, *Phys. Rev. Lett.* 64 (18): 2206 – 2209.
- Wen, X. G. (1991). Gapless Boundary Excitations in the Quantum Hall States and in the Chiral Spin States, *Phys. Rev. B* 43 (13): 11025 – 11036.
- Xia, F.; Farmer, D. B.; Lin, Y.-M.; Avouris, P. (2010). Graphene Field-Effect Transistors with High On/Off Current Ratio and Large Transport Band Gap at Room Temperature, *Nano Lett.* 10 (2): 715 – 718.
- Yang, L.; Cohen, L. M.; Louie, G. S. (2008). Magnetic Edge-State Excitons in Zigzag Graphene Nanoribbons, *Phys. Rev. Lett.* 101 (18): 186401 – 186404.
- Zhang, Y.; Tan, Y. W.; Stormer, H. L.; Kim, P. (2005). Experimental Observation of the Quantum Hall Effect and Berry's Phase in Graphene, *Nature* 438: 201 – 204.
- Zhang, Y.; Jiang, Z.; Small, J. P.; Purewal, M. S.; Tan, Y.-W.; Fazlollahi, M.; Chudow, J. D.; Jaszczak, J. A.; Stormer, H. L.; Kim, P. (2006). Landau-Level Splitting in Graphene in High Magnetic Fields, *Phys. Rev. Lett.* 96 (13): 136806 – 136809.
- Zhang, Y.; Tang, T.-T.; Girit, C.; Hao, Z.; Martin, M. C.; Zettl, A.; Crommie, M. F.; Shen, Y. R.; Wang, F. (2009). Direct Observation of a Widely Tunable Bandgap in Bilayer Graphene, *Nature* 459: 820-823.
- Zhou, J.; Wang, Q.; Sun, Q.; Chen, X. S.; Kawazoe Y.; Jena P. (2009). Ferromagnetism in Semihydrogenated Graphene Sheet, *Nano Lett.* 9 (11): 3867 – 3870.



Physics and Applications of Graphene - Theory

Edited by Dr. Sergey Mikhailov

ISBN 978-953-307-152-7

Hard cover, 534 pages

Publisher InTech

Published online 22, March, 2011

Published in print edition March, 2011

The Stone Age, the Bronze Age, the Iron Age... Every global epoch in the history of the mankind is characterized by materials used in it. In 2004 a new era in material science was opened: the era of graphene or, more generally, of two-dimensional materials. Graphene is the strongest and the most stretchable known material, it has the record thermal conductivity and the very high mobility of charge carriers. It demonstrates many interesting fundamental physical effects and promises a lot of applications, among which are conductive ink, terahertz transistors, ultrafast photodetectors and bendable touch screens. In 2010 Andre Geim and Konstantin Novoselov were awarded the Nobel Prize in Physics "for groundbreaking experiments regarding the two-dimensional material graphene". The two volumes *Physics and Applications of Graphene - Experiments* and *Physics and Applications of Graphene - Theory* contain a collection of research articles reporting on different aspects of experimental and theoretical studies of this new material.

How to reference

In order to correctly reference this scholarly work, feel free to copy and paste the following:

Duminda K. Samarakoon and Xiao-Qian Wang (2011). Structural and Electronic Properties of Hydrogenated Graphene, *Physics and Applications of Graphene - Theory*, Dr. Sergey Mikhailov (Ed.), ISBN: 978-953-307-152-7, InTech, Available from: <http://www.intechopen.com/books/physics-and-applications-of-graphene-theory/structural-and-electronic-properties-of-hydrogenated-graphene>

INTECH
open science | open minds

InTech Europe

University Campus STeP Ri
Slavka Krautzeka 83/A
51000 Rijeka, Croatia
Phone: +385 (51) 770 447
Fax: +385 (51) 686 166
www.intechopen.com

InTech China

Unit 405, Office Block, Hotel Equatorial Shanghai
No.65, Yan An Road (West), Shanghai, 200040, China
中国上海市延安西路65号上海国际贵都大饭店办公楼405单元
Phone: +86-21-62489820
Fax: +86-21-62489821

© 2011 The Author(s). Licensee IntechOpen. This chapter is distributed under the terms of the [Creative Commons Attribution-NonCommercial-ShareAlike-3.0 License](#), which permits use, distribution and reproduction for non-commercial purposes, provided the original is properly cited and derivative works building on this content are distributed under the same license.

IntechOpen

IntechOpen